

March 10, 2021

# Report on the Nuclear Magnetic Resonance Experiment

Marko Brnovic<sup>a,\*</sup>, Krzysztof Warmuz<sup>a</sup>

<sup>a</sup>New York University Abu Dhabi

## Abstract

In this experiment we conduct Nuclear Magnetic Resonance experiments to investigate the relaxation times of free-precessing protons in several organic compounds including mineral oils of ranging viscosity and water. For the spin-lattice relaxation times ( $T_1$ ) we used the inversion-recovery method. For the spin-spin relaxation times ( $T_2$ ) we used the Carr-Purcell and Meiboom-Gill methods to obtain a holistic comparison. For water we obtained  $T_1 = 2.4021 \pm 0.0007$  s and  $T_2 = 0.7124 \pm 0.0591$  s with the Carr-Purcell method, which is well within the acceptable range in literature, at room temperature. The values of  $T_1$  and  $T_2$  for light, heavy and extra heavy mineral oils were concordant with literature values, but the Meiboom-Gill sequence proved to be a more trustworthy method for finding  $T_2$ , with the exception of water. A simple one-dimensional analysis of an unknown sample was attempted. The information of the spin-lattice relaxation time was used to discover whether the unknown mixture was in fact a combination of light mineral oil and extra-heavy mineral oil. The study merely shows that a studying composite materials using effects of nuclear magnetic resonance, albeit challenging, is achievable. Moreover, the gyromagnetic ratio of a proton was determined to be  $42.934 \pm 0.430$  MHz T $^{-1}$ , which was less than 0.84% in discrepancy with the accepted value.

## 1. Introduction

### 1.1. Spin and magnetic moment

Since the development of modern physics at the turn of the 20<sup>th</sup> century many theories have been proved, disproved and upgraded. Above all, Quantum Mechanics has brought along most new concepts and phenomena. In particular, the principle of rotation or 'spin' being intrinsic to a fundamental particle became apparent [1]. Since it has no classical analogue and its closest 'relative' is angular momentum, it is most commonly associated with the overall angular momentum of a particle. Moreover, it is now well known that spin is a quantised elementary physical property whereby only some values of spin are allowed (integer and half-integer) [2]. In general, if a particle has spin  $S$ , the number of different states  $n$  that are allowed are given by

$$n = 2S + 1. \quad (1)$$

In other words, the existence of a spin 'breaks' the degeneracy of any energy level [3], since it can split into multiple different levels depending on the particle's spin. Of course, if the spin is 0, only one state is allowed and degeneracy is present.

Since the development of the Special Theory of Relativity and Particle Physics, a lot has been explained about spin and particles. In particular, according to relativistic quantum field theory it holds that all particles with half-integer spins are fermions, and those with integer spins are bosons [2]. Due to

the specific inconsistencies with the fermionic probability<sup>1</sup>, having two fermions in the same quantum state is not allowed in the current formulation of Quantum Mechanics, as dubbed by the Pauli exclusion principle [4]. This is an important concept when it comes to determining the overall spin of a composite particle, alongside with spin additivity<sup>2</sup>. In particular, suppose we want to know the spin of a particular nucleus. According to Quantum Field Theory, only constituents of the nucleus are protons and neutrons and they are both fermions [1]. That is to say, if there is an even number of protons or an even number of neutrons inside a nucleus at the same energy state, the combined spin of those protons or neutrons will always be zero. But if there is an odd number of either one, the spin for that energy state would be non-zero. Take, for example, Helium  ${}^2_4\text{He}$ . Since the constituents are two protons and two neutrons the overall spin will be zero. As a contrast, take Hydrogen  ${}^1_1\text{H}$  and Deuterium  ${}^1_2\text{H}$ . Hydrogen only has one proton whose spin is 1/2 and Deuterium has a proton and a neutron which (surprisingly) occupy the same spin state since it is more favourable so the overall spin is 1 [5].

Since spin is an analogue of angular momentum, it ought to have a direction, making it a vector physical quantity  $\mathbf{S}$ , with a magnitude which is an integer or half-integer and a unit vector in a particular direction. Furthermore, the particles we will be considering in this experiment are made up of other fundamental particles (such as quarks) which often carry some intrinsic charge in them (even if they are electrically neutral) [6] [7]. As

\*Main author

Email addresses: mb7187@nyu.edu (Marko Brnovic), ktw272@nyu.edu (Krzysztof Warmuz)

<sup>1</sup>In fact, wavefunction. Probability is an interpretation of the wavefunction.

<sup>2</sup>It is quantum-mechanical concept evident in classical mechanics. Since spins are vector quantities, they ought to be additive and the overall spin is the sum of individual constituents' spins.

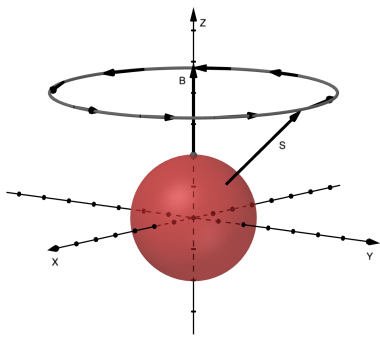


Figure 1: Precession of a model sphere of a nucleus around a constant magnetic field in the  $\hat{z}$  direction.

a consequence of that<sup>3</sup> these particles will have a magnetic moment [8] assigned to them which is determined by the relation

$$\mu = \gamma \mathbf{S} \quad (2)$$

Where  $\gamma$  is a constant for a particle which is called a gyro-magnetic ratio [9]. A dipole with a magnetic moment  $\mu$  in an external magnetic field  $\mathbf{B}$  has additional energy

$$\Delta U = -\mu \cdot \mathbf{B} \quad (3)$$

And a torque exerted on it

$$\tau = \mu \times \mathbf{B} \quad (4)$$

Which explains degeneracy breaking.

## 1.2. Painting a picture

Suppose we have a compound which is known to contain hydrogen. There is no physical reason why the spins of any two hydrogen nuclei should be the same [10]. Hence the orientation of each spin is random. However, if we apply a magnetic field in a region where this compound is placed, the magnetic moment of each nucleus will start precessing around this magnetic field [11], as dictated by the torque on them as shown by Figure 1.

In fact, the frequency of this precession is called the *Larmor Frequency*  $\omega_L$ . It holds that

$$\omega_L = \gamma |\mathbf{B}|. \quad (5)$$

The magnetic moment vector is bound to precess around the  $\mathbf{B}$  axis, and it can do so in two ways [12]. One is such that on average the spin vector is parallel and the other is such that it is antiparallel to the magnetic field. Since the former is much more energetically favourable and stable, the average particle in

our ensemble will have an *average magnetic moment* parallel to the magnetic field. For a large ensemble, the sum of these moments is called the magnetisation  $\mathbf{M}$ . Hence, in a constant, uniform magnetic field it holds that

$$\mathbf{M} \parallel \mathbf{B} \quad (6)$$

The property of magnetisation of non-zero spin particles in a uniform constant magnetic field and Larmor precession is essential in Nuclear Magnetic Resonance experiments.

## 1.3. RF pulse

It is conventional to make the  $\hat{z}$  and  $\mathbf{B}$  (hence the magnetisation) axes parallel to each other, even in the case of an actual experiment [13]. But if the magnetisation is just constant it does not tell us anything about the system. We must 'probe' the stable state somehow to obtain information from it. Suppose we apply another magnetic field perpendicular to the magnetisation vector. Since there is a torque now on the nuclei they will, in response to the new magnetic field, turn and thus magnetisation will rotate [14]. However, if we turn off the magnetic field, the magnetisation will return to the initial, energetically favourable state. So the reproducibility of this experiment is not compromised by the applied magnetic field.

The magnetic field which is commonly used in experiments like these is called an *Radio-frequency pulse* [15]. This is a polarised electromagnetic wave with the frequency corresponding to the radio-part of the EM spectrum which has the magnetic field component always pointing in the  $x$ - $y$  plane, with respect to the constant magnetic field axis. This is a way to 'probe' the magnetisation of the nuclei ensemble and an example of this is portrayed in Figure 2.

## 1.4. Detection

The key point from the rotation of the magnetisation vector is to notice that before the RF pulse, the magnetisation had no component in the  $x$ - $y$  plane. After the pulse, it is evident due to the rotation that that component is no longer zero [16]. Suppose we leave a solenoid next to our sample such that only the change in the  $x$ - $y$  plane is detected. This means that the planes where the coils of the solenoid lie is parallel to the  $x$ - $y$  plane [16]. When the magnetisation goes back to the equilibrium state, due to the movement of magnetic moment vectors a current would be induced in those coils. If the coil is connected to a recording device such as an oscilloscope, and the signal amplified, the oscilloscope would register a significant signal.

We previously saw why this technique encompasses the terms 'nuclear' and 'magnetic', but what about 'resonance'? It turns out that there is a reason the electromagnetic wave used is specifically in the radio spectrum. According to eq. (5), the Larmor precession frequency depends on the external magnetic field and inherent properties of the particle. Supposedly we know both of these two quantities and we can calculate the Larmor frequency. Then, if we set the RF pulse's frequency

<sup>3</sup>In fact, this is an occurrence when a classical phenomenon is translated in a quantum mechanical context.

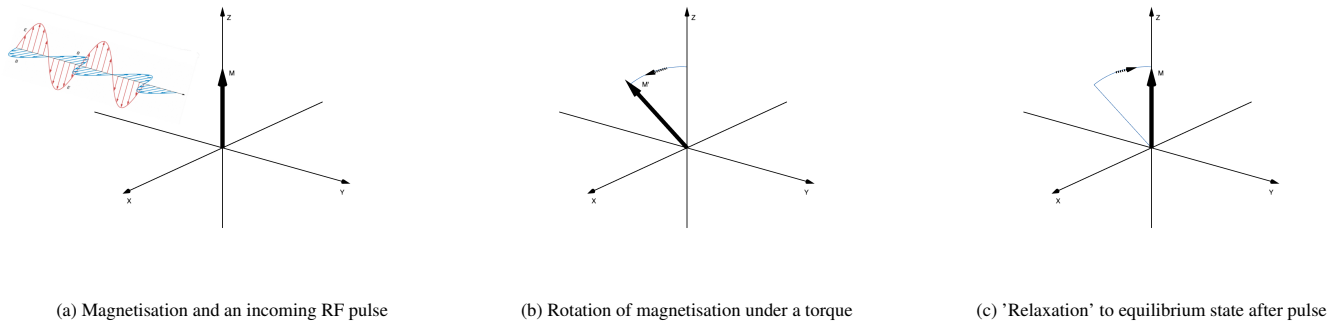


Figure 2: A magnetisation initially in the  $\hat{z}$  direction gets rotated to an angle due to an RF pulse, and relaxed back to equilibrium state

to match the Larmor frequency, the signal obtained in the detection coils will be the largest, due to resonance of the two frequencies. In modern instruments, resonance is imperative to obtain an optimal signal [16].

### 1.5. Relaxation

It is evident that under a change of magnetic field, the macroscopic magnetisation of the sample changes. In what way? Due to the fact that in most soft solids and liquids, the probability associated with a particular state is described by a Boltzmann distribution, the 'relaxation' of the magnetisation, or the process of returning magnetisation to the equilibrium position, can be modelled mathematically [17]. When doing an NMR experiment, one can distinguish between two types of relaxation.

#### 1.5.1. Spin-lattice relaxation

The Spin-Lattice relaxation occurs when a constant magnetic field is applied to a sample whose spins are randomly oriented<sup>4</sup> [18]. If, after a long time interval  $t \rightarrow \infty$  the magnetisation component in the  $\hat{z}$  axis is  $M_0$ , then the magnetisation in that axis, at any time  $t$  will be given by the equation

$$M_z(t) = M_0 \left(1 - e^{-\frac{t}{T_1}}\right) \quad (7)$$

Where  $T_1$  is a time constant specific to each particle in individual environments. That is, even if we are considering indistinguishable particles, due to the fact that they may be in different chemical environments, they may not have the same time constant  $T_1$ .

The extent and the speed of the change of magnetisation is governed by the random interatomic and intermolecular forces inside the sample. This is why this type of relaxation is called spin-lattice relaxation [18].

<sup>4</sup>This just means that no other magnetic field is applied before and that there is no reason for spins to be oriented in a particular way.

#### 1.5.2. Spin-spin relaxation

The spin-spin relaxation has to do with the response of the magnetisation of an ensemble to the incident weak oscillating magnetic field - our RF pulse [19]. Since the magnetisation gets rotated to obtain a component in the  $x$ - $y$  plane, after stopping the RF pulse that magnetisation has to revert back to the equilibrium position. Unlike the spin-lattice relaxation, this process has two components - one for the  $x$  and one for the  $y$  axis. It holds that the respective magnetisation components in most soft solids and liquids will follow the model [11]

$$\begin{cases} M_x(t) = -M_0 \cos(\omega_L t) e^{-\frac{t}{T_2}} \\ M_y(t) = M_0 \sin(\omega_L t) e^{-\frac{t}{T_2}} \end{cases} \quad (8)$$

Where  $T_2$  is the corresponding time constant for the spin-spin relaxation.

The two time constants  $T_1$  and  $T_2$  are some of the most studied parameters inside an NMR experiment [16]. If they are known they can be used to test purity and the composition of samples.

### 1.6. Free Induction Decay

When at resonance, suppose we apply an RF pulse which flips the magnetisation vector by  $90^\circ$ . Then, the signal picked up by the solenoid will be strongest since this conformation would take the longest to return to the equilibrium state. Over time, this signal decreases (to zero when the magnetisation and the magnetic field are fully aligned again). The signal will oscillate (due to the Larmor precession in the  $x$ - $y$  plane), but the amplitude of the signal (envelope) will follow an exponential pattern. On the oscilloscope, this envelope curve is called the Free Induction decay curve [11] and it has been portrayed in Figure 3.

### 1.7. Fast Fourier Transform

The composition of a sample can be confirmed using the time constants, but observing peaks can sometimes be very difficult when there are several compounds used inside the sample (see Figure 22). The resulting signal does not have well-resolved peaks and it is an inconclusive test as to how

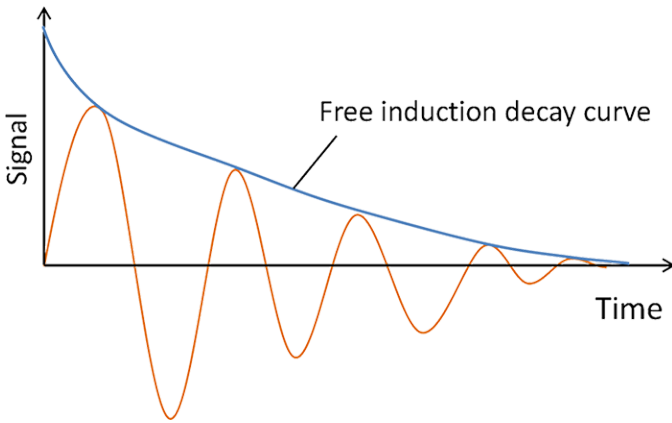


Figure 3: Free Induction Decay curve of an NMR signal

many different environments there are for the particle we are doing an NMR experiment with.

In order to distinguish two different signals (coming from particles in two different environments), it is much more useful to transfer the graph from time-space to frequency-space where the two peaks will be visibly resolved. This is called a Fast Fourier Transform (see Figure 23). By moving from time domain to frequency domain it shows different Larmor frequencies [20]. But since we know that the Larmor frequency depends on the chemical environment and the value of the magnetic field, and the magnetic field is constant, it must hold that these different Larmor frequencies imply different chemical environments<sup>5</sup>. Using this technique, we can see much clearer as to how many environments there are for a particular particle (say, a proton).

## 2. Methodology

### 2.1. Experimental set-up

We used a Textronix TBS1102 Oscilloscope with a PS2-A TeachSpin pulsed NMR device which included a permanent Neodymium (NdFeB) magnet, a control panel for magnetic field gradients and the mainframe which included a pulse receiver, pulse synthesiser, pulse programmer and a lock-in/field sweep controllers<sup>6</sup> (Figure 5).

The permanent magnet (Figure 4a) had to be rested at a constant temperature which was ensured by the laboratory's air conditioning system. The nominal strength of the uniform magnetic field was  $0.50 \pm 0.01$  Tesla and the region of homogeneity was  $0.125\text{cm}^3$ . The region of homogeneity coincided with receiver coils and the opening for the sample (Figure 4b). Furthermore, around the sample there were tuning capacitors which would serve to set the optimal frequency of sample coils: one that would match the one from the RF pulse, so

that there is resonance [21]. Before each experiment, a sample probe would be used to tune the circuit to optimal frequency for a specific RF pulse, to achieve resonance. The samples were consistently placed in 125mL volume inside a vial, which would then be sealed and lowered to an appropriate height inside the opening within the magnet.

The controller (Figure 4c) was used to adjust the magnetic field gradients in the  $x$ ,  $y$  and  $z$  directions during the 1-dimensional imaging experiment. During the relaxation times testing, they were all set to zero so that the magnetic field vector is uniform and always coincides with the  $z$  axis.

#### 2.1.1. Resonance

All of the RF pulses were calibrated to the frequency range  $21.467 \pm 0.01$  MHz. This frequency range gave us a consistently strong signal in all samples we used and hence we concluded that the Larmor frequency of protons of all of our samples was in this range.

### 2.2. Method for calculating $T_1$

For calculating  $T_1$  we used a *Inversion-Recovery* method [22]. It begins by applying an RF pulse which would rotate the magnetisation of our sample by  $180^\circ$ . This is accomplished by adjusting the time interval of the 'A Pulse' on the pulse programmer module. During the  $180^\circ$  pulse, no FID is registered since there is no magnetisation in the  $x$ - $y$  plane. Another  $90^\circ$  pulse (called the 'B Pulse') is applied some time  $\tau$  (that is also varied on the pulse programmer) after the  $180^\circ$  pulse. The magnitude of the voltage on the oscilloscope during the FID signal of the  $90^\circ$  pulse would indicate the amplitude of magnetisation. According to equation (7), when varying  $\tau$  and plotting the voltage amplitude against it, the graph should follow an exponential fit. Thus the amplitudes were taken for several values of  $\tau$  and plotted against an exponential line optimised for best fit in Python: Anaconda Notebook. Since the magnetisation is reversed fully by the A pulse, the initial magnetisation after the pulse is of the same magnitude as that of the equilibrium magnetisation, but opposite sign. Applying these initial conditions to the differential equation that yielded (7), we obtain a somewhat similar equation:

$$M_z(t) = M_0 \left( 1 - 2e^{-\frac{t}{T_1}} \right). \quad (9)$$

From (9) we can conclude that there exists a  $\tau_0$  such that  $M_z(\tau_0) = 0$ . It further holds that

$$T_1 = \frac{\tau_0}{\ln 2}. \quad (10)$$

Thus, the spin-spin relaxation time was always calculated using formula (10), whereby the interception of the line of best fit was divided by  $\ln 2$ .

<sup>5</sup>'Chemical environment' is a widely used term which could signify a specific compound or even a region within a compound.

<sup>6</sup>These were not used throughout the experiment

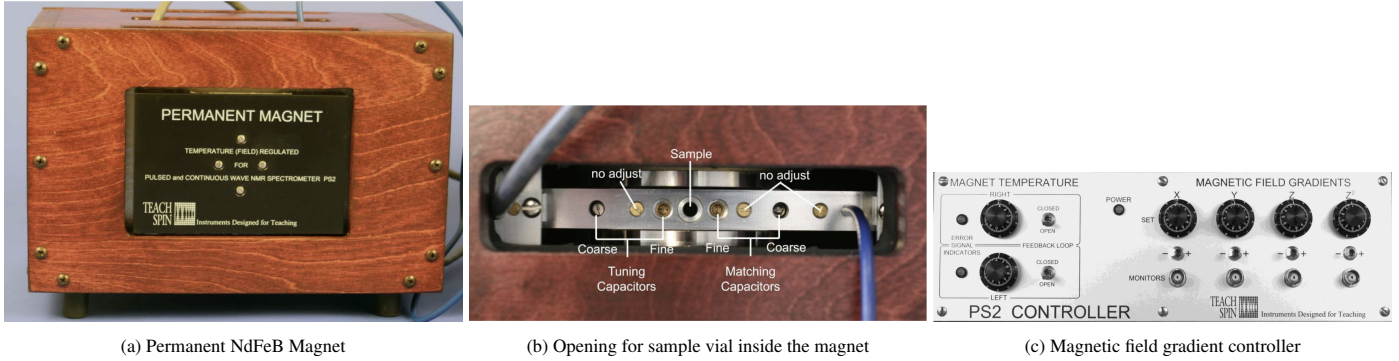


Figure 4: Different components of the PS2-A Magnet

### 2.3. Methods for calculating $T_2$

$T_2$  presents a more challenging measurement due to the fact that the relaxation due to spin arrangement is a more difficult concept to quantitatively describe compared to the relaxation due to the thermodynamic equilibrium ( $T_1$ ). This is why we used two different methods: to obtain a more holistic study of the spin-spin relaxation and to compare which experimental method would provide a result closer to a literature-acceptable value.

### 2.4. Purcell-Carr method

The Purcell-Carr method is methodologically simpler of the two: it consists of applying a  $90^\circ$  pulse, followed by many  $180^\circ$  pulses (we used 100 in this experiment). During the  $90^\circ$  pulse, the magnetisation fully gets rotated to the  $x$ - $y$  plane. However, as it is relaxing, a  $180^\circ$  pulse will rotate it fully again after which an 'echo' signal is observed [23]. The amplitude of this echo signal at a particular time is characterised by the spin-spin relaxation time constant. In particular, when we apply a multitude of  $180^\circ$  pulses, the resulting graph (Figure 8) can clearly show the decreasing exponential nature of the echo signal amplitude. Furthermore, if the shape of the graph is unexpected it can also allude to the fact that the set-up may be faulty.

The line of best fit was plotted against the maxima of each peak in an interval of  $\approx 40$  points. This ensured we preserved the nature of the graph and improved our analysis largely since there was very little deviation of the best-fit line from the maxima of the successive FID's, which is testified by the low chi-squared values (Table 2).

Albeit methodologically undemanding, the Carr-Purcell method has some drawbacks. In particular, since it is challenging to achieve a perfect-zero signal corresponding to a  $180^\circ$  pulse. There will be a mistake almost always (a couple of degrees) regarding the pulse. When applying the same pulse in a sequence of a total 100 pulses in a short time interval (typically 2 ms), that mistake accumulates and the resulting misalignment of the magnetisation after just a few pulses will be tens of degrees. This may drastically affect the shape of the exponential, and hence the time constant, so we made sure to

calibrate our equipment to ensure a near-perfect  $180^\circ$  pulse.

Moreover, to account for imperfect inversions of spin and noise, we have made sure to plot the lines of best fit as either

$$\text{a) Simple exponential: } f(t) = Ce^{-\frac{t}{T_2}}$$

Or

$$\text{b) Modified exponential: } f(t) = C_1 e^{-\frac{t}{T_2}} + C_2.$$

The reported data contains time constants obtained in both analyses, they are compared to literature values to deduce which method is more reliable for recovering accurate values of  $T_2$ .

### 2.5. Meiboom-Gill method

The second slightly more complicated method for calculating the spin-spin relaxation time is the Meiboom-Gill method. Here, we are also applying a sequence of  $90^\circ$  and  $180^\circ$  pulses, but this time with only one  $180^\circ$  pulse. Then, we measure the amplitude of the echo signal for several different  $\tau$  - time in between two pulses. The corresponding plot of amplitude versus  $\tau$  should give us an exponential decrease whose time constant is  $T_2$  [24]. This method resembles the inversion-recovery method in the sense that a similar line of code was used to plot a line of best fit. That being said, it is important to note that the order of signals is reversed and the dependent variable is not the amplitude of the  $90^\circ$  signal, but that of the echo, so the two analyses represent two different time constants.

### 2.6. One-Dimensional imaging

We had mixed equal amounts of light and extra-heavy mineral oil (since they gave us the most distant values of  $T_1$  out of all mineral oils) and attempted an inversion recovery method. The study consisted of observing individual peaks from a composite FID resulting from the sample and plotting the maxima against time to search for relaxation time (time constant corresponding to the decaying exponential of amplitude) for each peak and identify the sample with the nearest  $T_1$ .

It is worth noting that extensive amount of research has not been done for this section, as it was intended to be a pioneering

study. We assumed that the FID signal would be simply a superposition of the two signals which could be resolved and differentiated between. With this assumption, we took the first two peaks present in the FID signal to be the signals corresponding to each of the oils within the sample.

### 2.7. Gyromagnetic ratio of the proton

As mentioned in section 2.1 and subsection 2.1.1, we have deduced the values for the strength of the magnetic field and the Larmor precession frequency of protons, along with their respective uncertainties. Thus, the gyromagnetic ratio was calculated (according to equation 5) to be

$$\gamma_P = \frac{\omega_L}{B} \quad (11)$$

The obtained value was compared against a widely accepted one by means of a *t*-test, and an estimate of the percentage error. A more comprehensive explanation on our error analysis can be found in Appendix B.

## 3. Results

The Results section contains detailed description of relaxation times of each sample. For a summary, refer to table 1.

### 3.1. Light Mineral Oil

#### 3.1.1. Spin-lattice relaxation time

For light mineral oil, the obtained value for  $T_1$  was  $0.0664 \pm 0.0007$  s, as shown by the interception of the x axis corresponding to Figure 6.

#### 3.1.2. Spin-spin relaxation time

For the Carr-Purcell method, the simple exponential function yielded a time constant  $T_2 = 0.0646 \pm 0.0045$  s, as shown by Figure 7. On the other hand, the modified exponential function yielded a time constant  $T_2 = 0.0480 \pm 0.0017$  s, as shown by Figure 8. The Meiboom-Gill method yielded a value of  $0.0428 \pm 0.0055$  s for  $T_2$ , as shown by Figure 9.

### 3.2. Heavy Mineral Oil

#### 3.2.1. Spin-lattice relaxation time

For heavy mineral oil, the obtained value for  $T_1$  was  $0.050 \pm 0.0007$  s, as shown by the interception of the x axis corresponding to Figure 10.

#### 3.2.2. Spin-spin relaxation time

For the Carr-Purcell method, the simple exponential function yielded a time constant  $T_2 = 0.0534 \pm 0.0069$  s, as shown by Figure 11. On the other hand, the modified exponential function yielded a time constant  $T_2 = 0.0429 \pm 0.0013$  s, as shown by Figure 12. The Meiboom-Gill method yielded a value of  $0.0367 \pm 0.0045$  s for  $T_2$  of heavy mineral oil, as shown by Figure 13.

### 3.3. Extra-Heavy Mineral Oil

#### 3.3.1. Spin-lattice relaxation time

For extra heavy mineral oil, the obtained value for  $T_1$  was  $0.0418 \pm 0.0007$  s, as shown by the the interception of the x axis corresponding to Figure 14.

#### 3.3.2. Spin-spin relaxation time

For the Carr-Purcell method, the simple exponential function yielded a time constant  $T_2 = 0.0293 \pm 0.027$  s, as shown by Figure 15. On the other hand, the modified exponential function yielded a time constant  $T_2 = 0.0351 \pm 0.008$  s, as shown by Figure 16. The Meiboom-Gill method yielded a value of  $0.0263 \pm 0.0072$  s for  $T_2$ , as shown by Figure 17.

### 3.4. Water

#### 3.4.1. Spin-lattice relaxation time

For water, the obtained value of  $T_1$  was  $2.4021 \pm 0.0007$  s, as shown by the interception of the x axis corresponding to Figure 18.

#### 3.4.2. Spin-spin relaxation time

For the Carr-Purcell method the simple exponential function yielded a time constant  $T_2 = 0.7119 \pm 0.159$  s, as shown by Figure 19. On the other hand, the modified exponential function yielded a time constant  $T_2 = 0.5054 \pm 0.0055$  s, as shown by Figure 20. The Meiboom-Gill method yielded a value of  $0.0835 \pm 0.0436$  s for  $T_2$ , as shown by Figure 21.

### 3.5. Tables of Results

In order to represent the results in the most compact manner, we present below a comprehensive table of results for all relaxation time measurements (Table 1). A chi-squared analysis was also carried out for each of the measurements. The chi-squared results are presented below (Table 2).

The chi-squared values for Car-Purcell simple exponential method appeared higher than for other methods, however their values got mitigated by the large (100) number of fitted points. The values for Car-Purcell exponential plus constant have acceptable values of chi-squared for the number of data points, which may suggest over-fitting. Overall, all the fit probabilities as derived by chi-squared were within no more than 0.1% from 1.

### 3.6. 1-Dimensional NMR imaging

We have recovered two spin-lattice relaxation times resulting from this study. The relaxation time corresponding to the first peak of the composite FID was found to be  $0.0131 \pm 0.0142$  s while the second one was found to be  $0.0198 \pm 0.0285$  s, according to the inversion - recovery method. They were in the same order of magnitude as compared to the actual  $T_1$  values obtained from individual studies, but varied from them for more than 200% in both cases.

Furthermore, the FFT of the composite FID resolved two separate peaks in the frequency-space, one at 3.7 kHz and another at 7.7 kHz (Figure 23).

Table of Results				
	Light	Heavy	Extra Heavy	Water
$T_1/\text{s}$	$0.0664 \pm 0.0007$	$0.0505 \pm 0.0007$	$0.0418 \pm 0.0007$	$2.4021 \pm 0.0007$
$T_2/\text{s}$ (Carr-Purcell, Simple Exponential)	$0.0646 \pm 0.0045$	$0.0534 \pm 0.0069$	$0.0293 \pm 0.0027$	$0.7119 \pm 0.0591$
$T_2/\text{s}$ (Car-Purcell, Modified Exponential)	$0.0480 \pm 0.0017$	$0.0429 \pm 0.0013$	$0.0351 \pm 0.0008$	$0.3203 \pm 0.0055$
$T_2/\text{s}$ (Meiboom Gill)	$0.0428 \pm 0.0055$	$0.0367 \pm 0.0045$	$0.0263 \pm 0.0072$	$0.0472 \pm 0.0436$

Table 1: Summarised table of results for relaxation times of all samples

Table of Chi-Squares				
	Light	Heavy	Extra Heavy	Water
$T_1/\text{s}$	0.073	0.001	0.073	0.158
$T_2/\text{s}$ (Carr-Purcell, Simple Exponential)	1.594	2.881	5.235	0.093
$T_2/\text{s}$ (Car-Purcell, Modified Exponential)	0.125	0.639	1.805	11.895
$T_2/\text{s}$ (Meiboom Gill)	0.012	0.095	0.130	0.999

Table 2: Summarised table of results for Chi-squared valued of all samples

### 3.7. Gyromagnetic ratio of the proton

The obtained value for the gyromagnetic ratio of the proton was

$$\gamma_P = 42.934 \pm 0.430 \text{ MHz T}^{-1}. \quad (12)$$

The t-test yielded a value of

$$t \approx 0.8295. \quad (13)$$

Which shows that the values are concordant to approximately 80% confidence interval.

The estimate of the percentage error was

$$\Delta p \approx 0.837\%. \quad (14)$$

## 4. Conclusions

We have presented both spin-spin and spin-lattice relaxation times of three different mineral oils and water. The spin-inversion method was overall effective and easy to run. The Carr-Purcell method yielded very good results even for water, despite being suggested to heavily accumulate the error [25]. Finally, the Meiboom-Gill method gave answers in good ranges for every sample, except water. The answer was of the correct order of magnitude, but heavily underestimated the real value. We believe this may have happened due to the impurities that were present in the water, since the vial has been refilled several time due to condensation on its sides.

Overall, for mineral oils, the values obtained were within the range of previously reported values in literature [25], although it seems like we conducted a first-time study for some of the samples, including extra heavy mineral oil. Since the

extra-heavy mineral oil is chemically similar to light and heavy mineral oils, it was expected that their relaxation times were comparable, and of the same order of magnitude which was confirmed. Moreover, for the spin-spin relaxation time, the more appropriate method was proven to be Meiboom-Gill since it reproduced results closer to the ones as seen in literature [25].

The fit curves for the data points appeared reliable and with good chi-squared probabilities, except the measurement of  $T_1$  for heavy oil, where first two data points had to be removed. The adjustment of exponential plus constant function when applied Carr-Purcell may suggest over-fitting, however still yields results within reasonable range.

When reporting errors for the spin-lattice relaxation time, an assumption was made that the line of best fit is optimal and as such the only uncertainty stems from the apparatus. This was an over-idealisation which manifested itself in a way that the standard error was deemed to be less significant than what it should have been. In order to improve error analysis for  $T_1$  one must also consider the  $\chi^2$  parameter of the line of best fit. When incorporating this into the analysis, one may obtain a result which is close to the actual value of  $T_1$  or within one standard deviation of the data.

The Meiboom-Gill method for water was surprisingly ineffective and consistently produced results which do not agree with literature values. The curve (Figure 21) had a large amount of outlier points and it did not seem as if the optimal fit was a decaying exponential, but a half-Gaussian distribution. The reason why we had not plotted any other curve onto the data we got was that there was no physical support to the theory

that the line of best fit should be anything but an exponential. Furthermore, we would not be able to extract information such as the relaxation time since a new theory would have to be in place in order to qualitatively describe this result. We suspect that the reason for the inefficiency was misalignment of the magnetic field gradients since we had to recalibrate them for the one-dimensional NMR imaging study.

The Carr-Purcell method showed to be extremely effective when we were able to produce a  $180^\circ$  pulse (see Figure 19). It produced relatively very low standard errors resulting from line of best fit<sup>7</sup>, which alludes to the fact that even an imperfect sequence of  $180^\circ$  pulses produces a near-perfect exponential decay. The discrepancy between the results obtained by the Carr-Purcell method and widely accepted ones is likely attributed to the imperfection of the  $180^\circ$  pulse or the uncertainty in the readings of the oscilloscope.

The NMR Fourier spectra of double sample containing light and extra-heavy mineral oil showed two distinct frequency peaks, proving multiple proton environments as the sources of resonance. The main conclusion from the one-dimensional imaging experiment was that resolving a peak coming from multiple samples proved to be an arduous task, for both interpretation and analysis. What could have helped with this problem is getting a more powerful oscilloscope, since the one used in this study was limited to 1GS/s. As for the interpretation, further study of composite FID curves is required to fully understand the various peaks which occur, and how to manipulate them to obtain valuable information such as individual relaxation times.

The data was taken at standard laboratory temperature - around  $20^\circ\text{C}$ . That being said, the laboratory temperature was not varied in this interval, which makes our study reproducible and consistent in two ways. The first is that the variation of temperature will highly likely affect the magnet and hence the magnetic field strength, which could lead to inconclusive results since they would not be reproducible. Secondly, all relaxation times were measured at the same temperature. In case the sample temperature was varied, the thermodynamic equilibrium of collective magnetisation would have been shifted, and hence the relaxation times would change accordingly. This change is, in fact, drastic - which is why any discrepancy of obtained result with respect to an accepted value is expected and tolerable - and a value is only considered acceptable at a specified temperature.

In order to do a more holistic study which would include a more complex error analysis and trustworthy results, reproduction of the above results is necessary at a higher resolution, and for a larger sample. A possible extension of this project is constructing highly sensitive receiver coils which could obtain an NMR signal in the Earth's magnetic field or lower magnetic

fields than the one used in this experiment.

Furthermore, for a one-dimensional imaging study, increasing the magnetic field gradient may result in a greater resolution in peak-resolving. A greater magnetic field with a smaller uncertainty may improve the accuracy of the calculation of the gyromagnetic ratio and the peak resolution in general.

## 5. Acknowledgments

We thank professor Francesco Arneodo and instructor Osama Fawwaz for their helpful instruction and support throughout this project.

## References

- [1] William Rarita and Julian Schwinger. On a theory of particles with half-integral spin. *Physical Review*, 60(1):61, 1941.
- [2] Wolfgang Pauli. The connection between spin and statistics. *Physical Review*, 58(8):716, 1940.
- [3] JM Jauch and EL Hill. On the problem of degeneracy in quantum mechanics. *Physical Review*, 57(7):641, 1940.
- [4] Wolfgang Pauli. Pauli exclusion principle. *Naturwiss*, 12:741, 1924.
- [5] GM Murphy and Helen Johnston. The nuclear spin of deuterium. *Physical Review*, 46(2):95, 1934.
- [6] Paul Adrien Maurice Dirac. A theory of electrons and protons. *Proceedings of the Royal Society of London. Series A, Containing papers of a mathematical and physical character*, 126(801):360–365, 1930.
- [7] James Chadwick. The neutron. *Proc. Roy. Soc.*, 142:1–25, 1933.
- [8] I Estermann, R Frisch, and O Stern. Magnetic moment of the proton. *Nature*, 132(3326):169–170, 1933.
- [9] Charles Kittel. On the gyromagnetic ratio and spectroscopic splitting factor of ferromagnetic substances. *Physical Review*, 76(6):743, 1949.
- [10] Erwin L Hahn. Spin echoes. *Physical review*, 80(4):580, 1950.
- [11] Erwin L Hahn. Nuclear induction due to free larmor precession. *Physical Review*, 77(2):297, 1950.
- [12] Erwin L Hahn. Free nuclear induction. *Physics Today*, 6(11):4–9, 1953.
- [13] Edwin D Becker. A brief history of nuclear magnetic resonance. *Analytical chemistry*, 65(6):295A–302A, 1993.
- [14] Joseph P Hornak. The basics of nmr, 1997. Cited on, page 9, 2017.
- [15] John D Roberts and Marjorie C Caserio. *Basic principles of organic chemistry*. WA Benjamin, Inc., 1977.
- [16] Peter J Hore. *Nuclear magnetic resonance*. Oxford University Press, USA, 2015.
- [17] Nicolaas Bloembergen, EM Purcell, and RV Pound. Nuclear magnetic relaxation. *Nature*, 160(4066):475–476, 1947.
- [18] Erwin L Hahn. An accurate nuclear magnetic resonance method for measuring spin-lattice relaxation times. *Physical Review*, 76(1):145, 1949.
- [19] R de L Kronig and CJ Bouwkamp. On the time of relaxation due to spin-spin interaction in paramagnetic crystals. *Physica*, 5(6):521–528, 1938.
- [20] Darien Gaudet and Hayden Savage. *Fourier Transform Spectroscopy*. PhD thesis, Worcester Polytechnic Institute, 1919.
- [21] EP Wagner. Understanding precessional frequency, spin-lattice and spin-spin interactions in pulsed nuclear magnetic resonance spectroscopy.
- [22] Gary A Lorigan, Robert E Minto, and Wei Zhang. Teaching the fundamentals of pulsed nmr spectroscopy in an undergraduate physical chemistry laboratory. *Journal of Chemical Education*, 78(7):956, 2001.
- [23] Terry Gullion, David B Baker, and Mark S Conradi. New, compensated carr-purcell sequences. *Journal of Magnetic Resonance (1969)*, 89(3):479–484, 1990.
- [24] Saul Meiboom and David Gill. Modified spin-echo method for measuring nuclear relaxation times. *Review of scientific instruments*, 29(8):688–691, 1958.
- [25] L Bianchini and L Coffey. Nmr techniques applied to mineral oil, water, and ethanol, 2010.
- [26] R. L. Driscoll and P. L. Bender. Proton gyromagnetic ratio. *Phys. Rev. Lett.*, 1:413–414, Dec 1958. doi: 10.1103/PhysRevLett.1.413. URL <https://link.aps.org/doi/10.1103/PhysRevLett.1.413>.

<sup>7</sup>Also likely attributed to the fact that errors get mitigated by a large sample of data points  $\approx 100$ .

## 6. Appendix A: Settings of the Apparatus

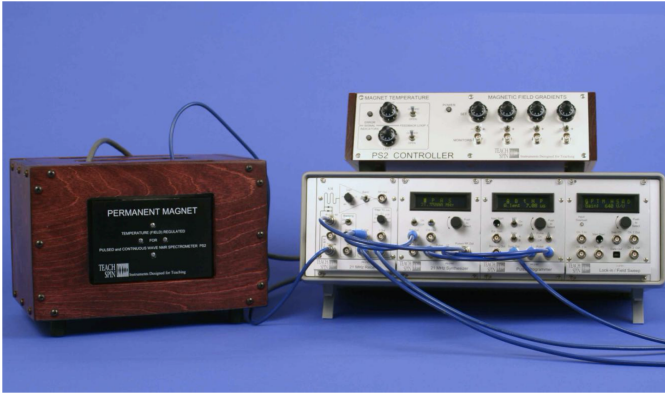


Figure 5: NMR Set-up (excluding the oscilloscope)

For light mineral oil, all data was taken at an RF frequency of 21.466 MHz. The length of the time interval which gave us a  $90^\circ$  pulse was  $3.44 \mu\text{s}$ . The length of the time interval which gave us a  $180^\circ$  pulse was  $6.90 \mu\text{s}$ . The repetition time of each succession of signal sequences was 0.80 s.

For heavy mineral oil, all data was taken at an RF frequency of 21.467 MHz. The length of the time interval which gave us a  $90^\circ$  pulse was  $3.66 \mu\text{s}$ . The length of the time interval which gave us a  $180^\circ$  pulse was  $7.30 \mu\text{s}$ . The repetition time of each succession of signal sequences was 0.90 s.

For extra-heavy mineral oil, all data was taken at an RF frequency of 21.467 MHz. The length of the time interval which gave us a  $90^\circ$  pulse was  $3.70 \mu\text{s}$ . The length of the time interval which gave us a  $180^\circ$  pulse was  $7.40 \mu\text{s}$ . The repetition time of each succession of signal sequences was 1.00 s.

For water, all data was taken at an RF frequency of 21.467 MHz. The length of the time interval which gave us a  $90^\circ$  pulse was  $3.00 \mu\text{s}$ . The length of the time interval which gave us a  $180^\circ$  pulse was  $6.94 \mu\text{s}$ . The repetition time of each succession of signal sequences was 0.80 s.

For light, heavy and extra-heavy mineral oils, the  $\tau$  increments for the Inversion-Recovery and Meiboom-Gill methods were set to be 6 ms. For water, due to the longer relaxation time, this was extended to 100 ms. For Carr-Purcell methods, we used various  $\tau$  values: 2ms, 1.5 ms, 1 ms and 0.5 ms to see if we get a different exponential fit corresponding to a particular  $\tau$ . The value of  $T_2$  seemed to be consistent regardless of the value of  $\tau$ .

The magnetic field gradient with respect to the y-axis was set to be  $\frac{\partial B}{\partial y} = 7.1 \mu\text{T/mm}$  in the one-dimensional NMR imaging study.

The complete set-up (with the exception of the oscilloscope) can be seen in Figure 5.

## 7. Appendix B: Error Analysis

The standard error of the spin-lattice relaxation time was calculated using the range of  $\tau_0$  which gave us the lowest signal, corresponding to the flipped magnetisation. This was taken to be  $\sigma_\tau = 0.5 \text{ ms}$ . Using (10), and the error propagation formula, the error was calculated using the formula

$$\sigma_{T_1} = \sigma_\tau \frac{\partial T_1}{\partial \tau} = \frac{\sigma_\tau}{\ln 2} \approx 0.72 \text{ ms}. \quad (15)$$

The standard error in the spin-spin relaxation time was calculated as following

$$\sigma_{T_2} = \frac{\sqrt{\sum (t_i - \bar{t})^2}}{n}. \quad (16)$$

Here,  $y$  represents the value of the line of best fit at time  $t$ . Furthermore,  $t_i$  is the obtained time data point corresponding to a value of voltage on an oscilloscope  $y_i$ . Lastly,  $t$  is the time on the line of best fit where  $y_i = y$  and  $n$  is the number of data points collected.

The standard error of the gyromagnetic ratio was calculated using the error propagation formula. Namely,

$$\sigma_{\gamma_p} = \sqrt{\sigma_\omega^2 \left( \frac{\partial \gamma_p}{\partial \omega} \right)^2 + \sigma_B^2 \left( \frac{\partial \gamma_p}{\partial B} \right)^2}. \quad (17)$$

And since  $\frac{\partial \gamma_p}{\partial \omega} = \frac{1}{B}$  and  $\frac{\partial \gamma_p}{\partial B} = -\frac{\omega}{B^2}$  it holds that

$$\sigma_{\gamma_p} = \sqrt{\frac{\sigma_\omega^2}{B^2} + \sigma_B^2 \frac{\omega^2}{B^4}}. \quad (18)$$

The  $t$ -value was obtained by the following formula

$$t = \frac{\gamma_p - \gamma'_p}{\sqrt{\sigma_{\gamma_p}^2 + \sigma_{\gamma'_p}^2}}. \quad (19)$$

Where  $\gamma'_p$  is the accepted value for the gyromagnetic ratio of the proton and  $\sigma_{\gamma'_p}$  its respective standard error [26].

The percentage error was calculated as

$$\Delta p = \frac{\gamma_p - \gamma'_p}{\gamma'_p} \cdot 100\%. \quad (20)$$

The chi-squared values in Table 2 were calculated using a script which used the following formula

$$\chi^2 = \sum_i \left[ \frac{y_i - \bar{y}}{\sigma_y} \right]^2 \quad (21)$$

Where  $\sigma_y = 0.04 \text{ V}$  and it comes from the natural uncertainty in the measurement of the voltage on the oscilloscope.

## 8. Appendix C: Figures

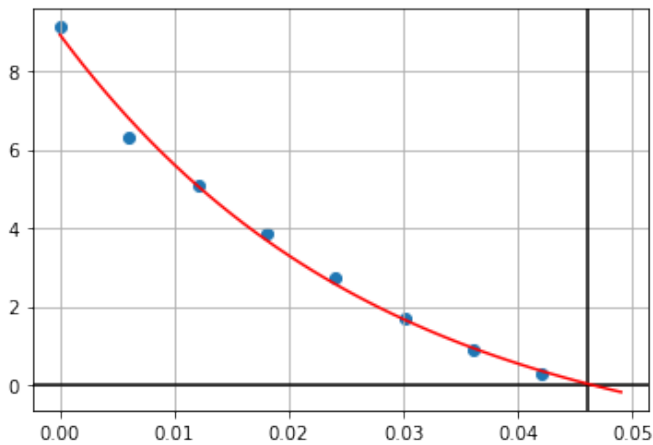


Figure 6: Inversion-Recovery method for light mineral oil

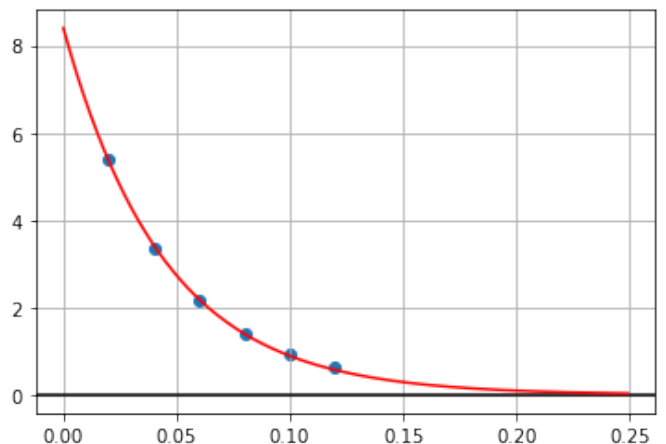


Figure 9: Plot of Meiboom-Gill method for light mineral oil

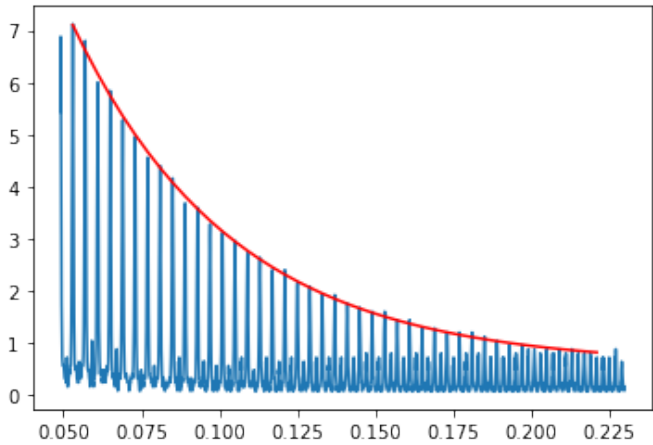


Figure 7: Plot of Carr Purcell method for light mineral oil

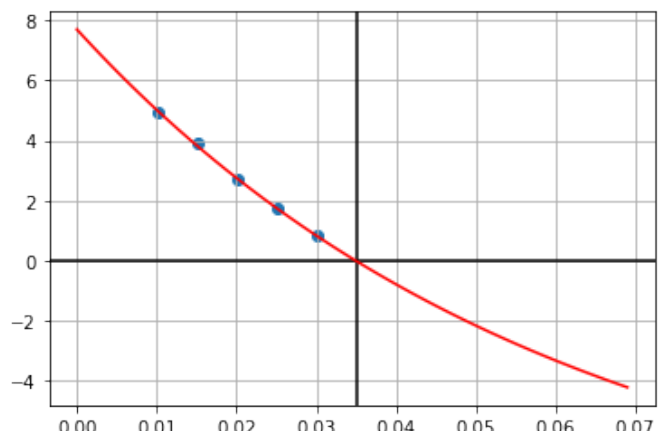


Figure 10: Inversion-Recovery method for heavy mineral oil

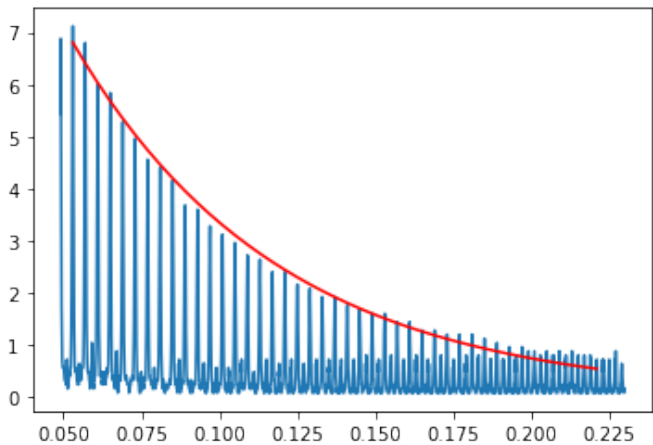


Figure 8: Plot of Carr-Purcell method for light mineral oil against a modified exponential

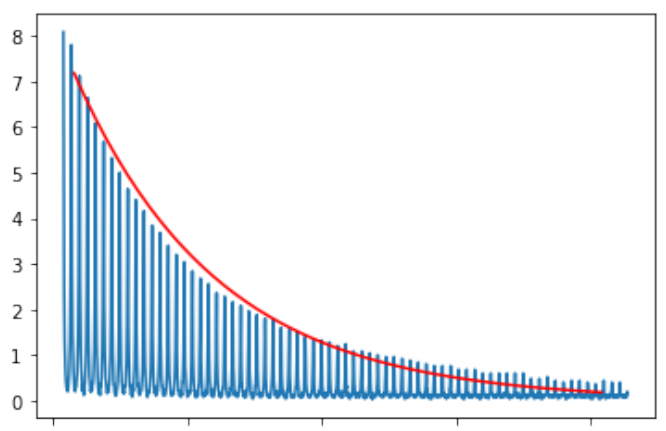


Figure 11: Plot of Carr Purcell method for heavy mineral oil

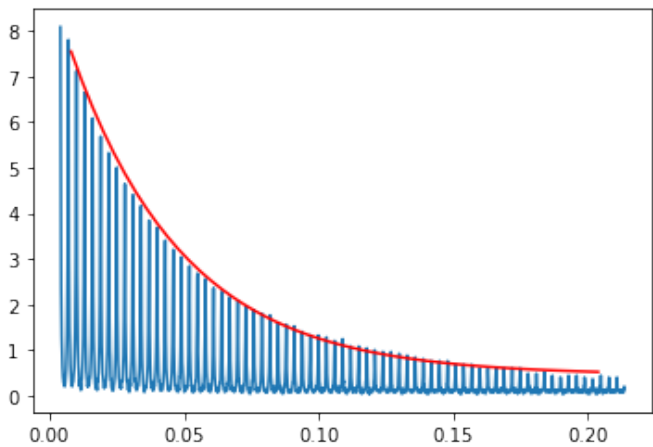


Figure 12: Plot of Carr Purcell method for heavy mineral oil against a modified exponential

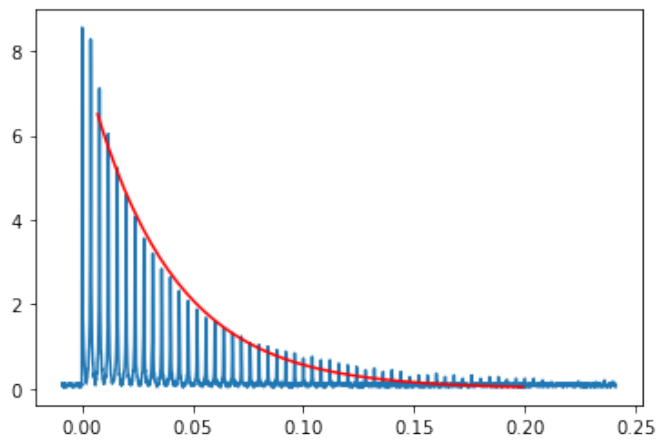


Figure 15: Plot of Carr Purcell method for extra heavy mineral oil

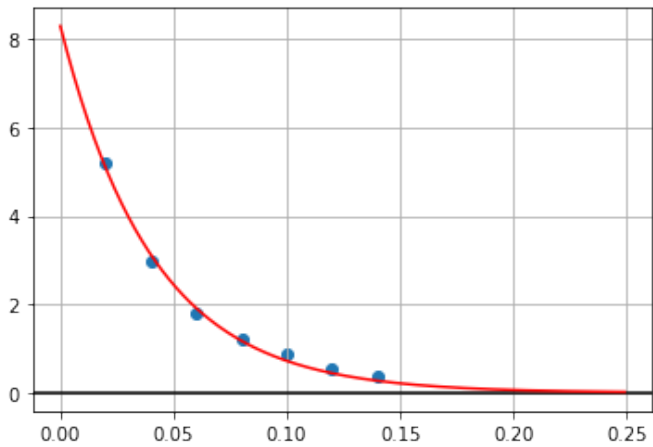


Figure 13: Plot of Meiboom-Gill method for heavy mineral oil

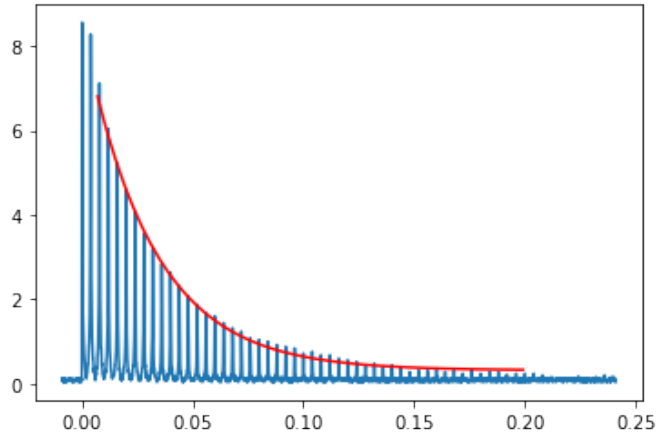


Figure 16: Plot of Carr Purcell method for extra heavy mineral oil against a modified exponential

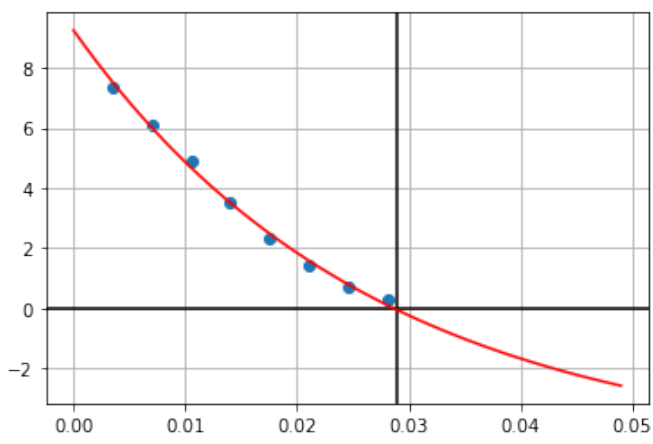


Figure 14: Inversion-Recovery method for extra heavy mineral oil

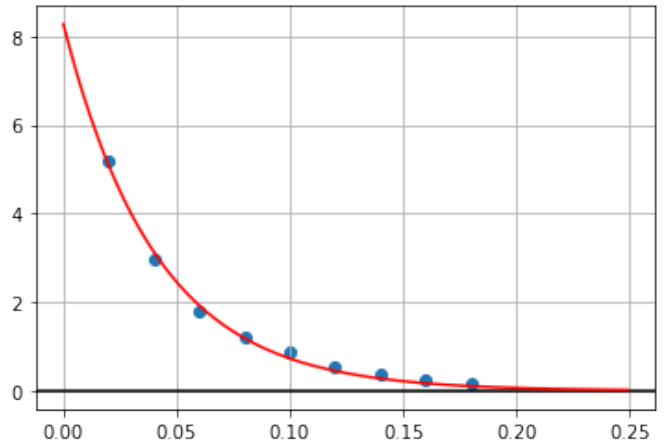


Figure 17: Plot of Meiboom-Gill method for extra heavy mineral oil

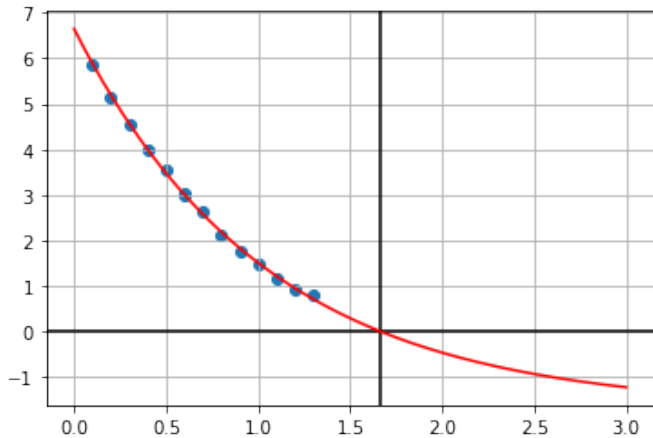


Figure 18: Inversion-Recovery method for water

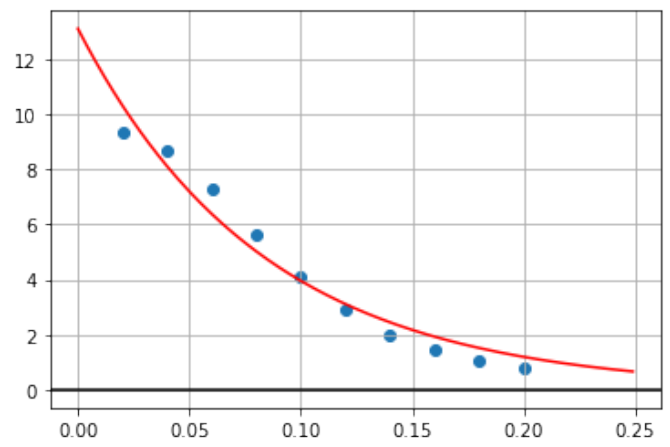


Figure 21: Plot of Meiboom-Gill method for water

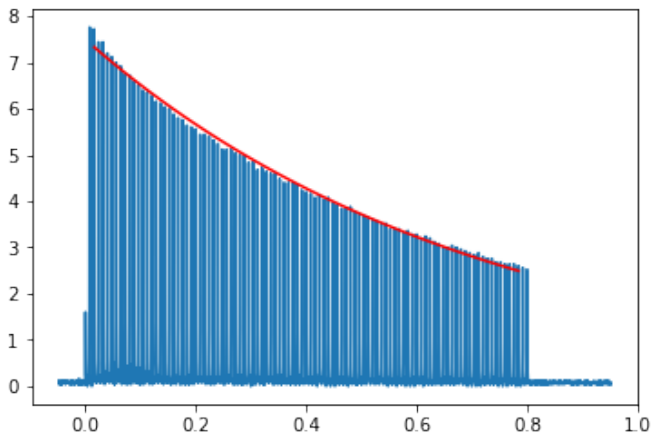


Figure 19: Plot of Carr Purcell method for water



Figure 22: An NMR signal resulting from a combination of light and extra-heavy mineral oil

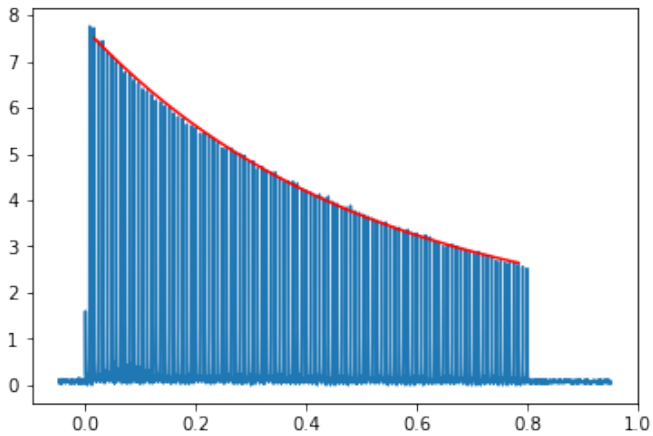


Figure 20: Plot of Carr Purcell method for water against a modified exponential

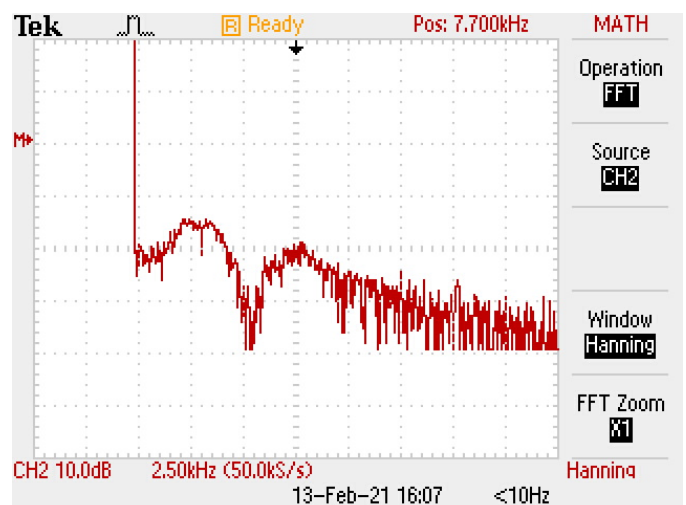


Figure 23: Fast fourier transform of the light oil - extra-heavy oil sample mixture showing two peaks, alluding to two different environments